Charge transfer in alkaline-earth metal Graphite Intercalation Compounds

Justine Zinni, Luigi Camerano, Lucie Speyer, Sébastien Cahen, Inass El Hajj, Mickaël Bolmont, Ghouti Medjahdi, Philippe Lagrange, Gianrico Lamura, Gianni Profeta, et al.

Charge transfer in alkaline-earth metal Graphite Intercalation Compounds

Justine Zinni[a], Luigi Camerano[b], Lucie Speyer[a], Sébastien Cahen[a], Inass El Hajj[a], Mickaël Bolmont[a], Ghouti Medjahdi[a], Philippe Lagrange[a], Gianrico Lamura[c], Gianni Profeta[b,d], Claire Hérold[a 1]

[a] IJL, Université de Lorraine, CNRS, 2 allée André Guinier, 54011 Nancy cedex, France

[b] Department of Physical and Chemical Sciences, University of L'Aquila, Via Vetoio, 67100 L'Aquila, Italy

[c] CNR-SPIN, Corso Perrone 24, 16152 Genova, Italy

[d] SPIN-CNR, University of L'Aquila, Via Vetoio 10, 67100 L'Aquila, Italy

Abstract

The charge transfer from a metal atom towards the carbon layers in first stage graphite intercalation compounds (GIC) is a fundamental issue to explain under which conditions superconductivity sets in and the electronic properties of such ground state. To study in detail the transfer process and its evolution as a function of the nature of the intercalated metal, and especially taking in consideration the interlayer distance, we performed detailed X-Ray Diffraction and Raman scattering measurements on very high-quality bulk intercalated CaC_6, SrC_6 and BaC_6 samples. We combined both the experimental results with detailed density functional theory calculations to give a coherent picture in which it is possible to follow the evolution of the charge transfer to the carbon layer in full agreement with the experimental data. The full comprehension of such mechanism remains a fundamental issue to explain the variation of the superconducting ground state in first stage GIC.

Keywords

Graphite intercalation compounds, alkaline-earth metals, charge transfer, X-ray diffraction, Raman spectroscopy, density functional theory calculations

1. Introduction

Graphite is a stacking of very robust and stable graphene layers which are linked together through weak Van der Waals interactions. This anisotropic structure remarkably allows the intercalation of numerous chemical species in its interlayer 2D spaces. This phenomenon is an interesting topotactic reaction [1] which necessarily involves a charge transfer between graphene layers and intercalated species. Among the electron donor elements, very electropositive metals are excellent candidates for intercalation since they give up very easily their valence electrons. This is the case for heavy alkali metals and to a lesser extent for lithium, alkaline-earth metals (M) and various lanthanides. The so-obtained graphite intercalation compounds (GIC) are said to be first stage when all the 2D intervals are occupied by a metallic plane. Their chemical formula is MC_8 for the largest intercalated atoms (K,

[1] claire.herold@univ-lorraine.fr
Institut Jean Lamour - UMR 7198 CNRS-Université de Lorraine
Campus ARTEM - 2 Allée André Guinier
B.P. 50840, 54011 Nancy Cedex, France

Rb, Cs) and MC_6 for all others. The intercalation of such mono-atomic layers of metal is always accompanied by an expansion along the c-axis of the graphene network. Moreover, during this reaction the filling of the π^* band of the graphene layers occurs due to the electron transfer from the metal to the graphene planes, which therefore become negatively charged [2]. This charge transfer leads to an increase in the in-plane carbon-carbon bond length which can be measured by the displacement of the X-ray *hk*0 reflections of the graphene planes [3].

Among the first stage GIC, CaC_6, SrC_6 and BaC_6 are particularly interesting, since they all turn out to be superconducting at the following respective critical temperatures: 11.5 K, 1.65 K and 0.065 K [4] [5] [6]. These observations thus triggered an intense experimental and theoretical research concerning these three lamellar compounds [7] [8] [9] [10] [11]. Some studies showed that the interlayer distance d_i of the graphene planes as well as the c-axis stacking sequence appear as parameters strongly correlated to the critical temperature of superconductivity, which is itself directly related to electron-phonon interactions.

The effective amount of charge transferred to C-layers heavily affects the electron-phonon scattering and the phonon spectrum. Such effects can be detected by measuring the variation of the peaks frequency and their linewidth in Raman spectra [12] [13] [14] [15] [16] [17] [18]. In the case of first stage GIC: two vibrational modes can be recognized, the so-called C_z and C_{xy} phonon modes. C_z one is originated from the C-M-C vibrational mode (only possible for 1st stage GIC) with displacements along the c-axis whereas C_{xy} is attributed to the coupling between graphene planes and intercalated layers characterized by in-plane (xy) vibrations. The first theoretical ab-initio calculation of GIC Raman response was performed by Saitta *et al.* [19]. They underlined the importance of non-adiabatic effects in CaC_6 to properly predict experimental phonon frequencies [20]. The same approach was then extended to all alkaline earth metal-based GIC to clarify the dependence between the Raman response and the interlayer distance d_i, eventually related to the GIC superconducting behavior [15].

In this paper, we present a detailed study of the charge transfer mechanism M↔C as a function of the interlayer distance in the three first stage alkaline-earth metal superconducting GIC CaC_6, SrC_6 and BaC_6. We will follow such mechanism by means of X-Ray Diffraction (XRD), Raman spectroscopy and Density Functional Theory (DFT) calculation, thus giving a coherent picture of such a mechanism. To this aim we synthesized very high purity bulk intercalated samples well detailed here below.

2. Experimental

2.1 Synthesis

In order to prepare bulk samples of MC_6 compounds, solid-liquid methods have to be used since the activity of the alkaline earth metal is higher in liquid medium than in vapour phase. The molten alloy method is the most efficient way to prepare CaC_6 samples, while SrC_6 and BaC_6 samples are prepared using the molten salts method.

2.1.1 Molten alloy method

The CaC_6 GIC was prepared using the molten alloy method [21]. All experiments have been made in a glove box under argon atmosphere which is purified of oxygen and water. Dendritic calcium (99.99% Sigma Aldrich) and lithium ingots (99.9% metal basis Sigma Aldrich) are used. Lithium is first purified by melting and removing impurities from its surface. Purified lithium and calcium are mixed in an 80at.% – 20at.% ratio in a stainless-steal reactor at 350°C to form a liquid alloy. After homogenisation by stirring, a platelet of pyrolytic graphite (PyroGraphite Comprimé Carbone Lorraine PGCCL) is immersed in the reactor thanks to a tungsten stick. The reactor is then hermetically closed with a Swagelok® plug, placed in stainless enclosure under argon and the intercalation reaction is performed in a furnace out of the glove box for 10 days at 350°C. After reaction, the recovery of the sample is performed inside the glove box. Further details are available in literature [21] [22].

2.1.2 Molten salts method

Regarding experimental difficulties for preparing bulk SrC_6 and BaC_6 GIC in Li-based molten alloys [23], the latter compounds have been synthesized using the molten salts method [24]. Once again, all the preparation is performed in a glove box under a purified argon atmosphere. An eutectic mixture of lithium chloride and potassium chloride (58.2%w-41.8%w) outgassed at 240°C under secondary vacuum is used as solvent. 2at.% of dendritic alkaline earth metals barium and strontium (99.99% Sigma Aldrich) are used without any further purification step and the same kind of platelet of pyrolytic graphite is chosen. Salts are introduced into a stainless-steel reactor and heated until the eutectic mixture is molten. Then, metallic element is plunged into this medium, which is stirred during 15 minutes for homogenization. The reactor is hermetically closed with a Swagelok® plug, placed in a stainless enclosure under argon and the reaction is performed into a rocking furnace out of the glove box for 12 days at 450°C. The recovery of the sample is performed in the glove box. Further details are available in literature [25] [26] [27] [28].

2.2 Characterization of GIC

2.2.1 Raman spectroscopy

Before Raman experiments, the surface of the samples has been cleaned by scrapping in glove box. Just a few minutes after scrapping, the samples are conditioned into a quartz cell under 100 mbar of helium gas and immediately after, Raman spectroscopy experiments have been performed with a Jobin Yvon Horiba LabRAM HR800 with a He/Ne laser source, the spectrometer operating with a wavelength of 632.8 nm. The power of the source is limited to 50% of its capacity (6,55 mW) in order to preserve the quality of the sample under irradiation. The focus is realized with a X50 lens and there are 1800 gaps in the grating. The spectra are recorded in three ranges: from 300 to 600 cm^{-1} for the C_z band, 1000 to 1700 cm^{-1} for the C_{xy} band and 2600 cm^{-1} to 2800 cm^{-1} to control the absence of any 2D band normally present in the case of pristine graphite samples.

2.2.2 X-Ray diffraction experiments

A piece of sample is cutted in the bulk intercalated material. Then, the measurements are performed with a Brüker D8 Advance diffractometer ($\lambda_{MoK\alpha1}$ = 70.926 nm) using a (θ, 2θ) configuration, Soller slit (1.2mm) and 2D LynxEye detector. Samples are conditioned under argon in Lindemann glass capillaries. Thanks to the extremely oriented nature of the pyrolytic graphite platelets, two sample configurations are possible so that 00*l* and *hk*0 reflections can be separately recorded by changing the sample orientation versus the X-ray beam: the 00*l* ones with the sample parallel to the beam; and the *hk*0 ones after a sample rotation of 90°. The latter are measured using diamond powder as internal standard.

3. Results and discussions

3.1 Crystallographic data

After reaction, samples are recovered in a glove box. CaC_6, SrC_6 and BaC_6 samples have a shiny silver color. Pictures of the samples can be retrieved in [4, 27, 28]. First, the 00*l* reflections are recorded in order to confirm the purity and the high quality of the prepared samples. Figure 1 shows the 00*l* diffractograms of the three CaC_6, SrC_6 and BaC_6 compounds. For each sample, a main set of well-defined and intense 00*l* peaks reveals the presence of a bulk single phase, *i.e.* first stage MC_6 compound. The corresponding repeat distances are 451 pm, 494 pm and 527 pm respectively in agreement with previous works [4] [27] [28]. Further details about the structure and composition of such GIC can be retrieved in [I. El Hajj et al. Carbon 213 (2023) 118310; S. Cahen et al. New J. Chem. 44 (2020) 10050-10055; S. Pruvost et al. Carbon 42 (2004) 2049-2056]"

It has been well established elsewhere that BaC_6 and SrC_6 crystallize in the hexagonal $P6_3/mmc$ space group with a AαAβAα… (A = graphene layer; α and β = barium or strontium layers) **c**-axis stacking (Fig. 2). The structure of CaC_6

on the other hand is different, with a AαAβAγ… (A = graphene layer; α, β and γ = calcium layers) **c**-axis stacking, leading to a rhombohedral *R*-3*m* space group (Fig. 2).

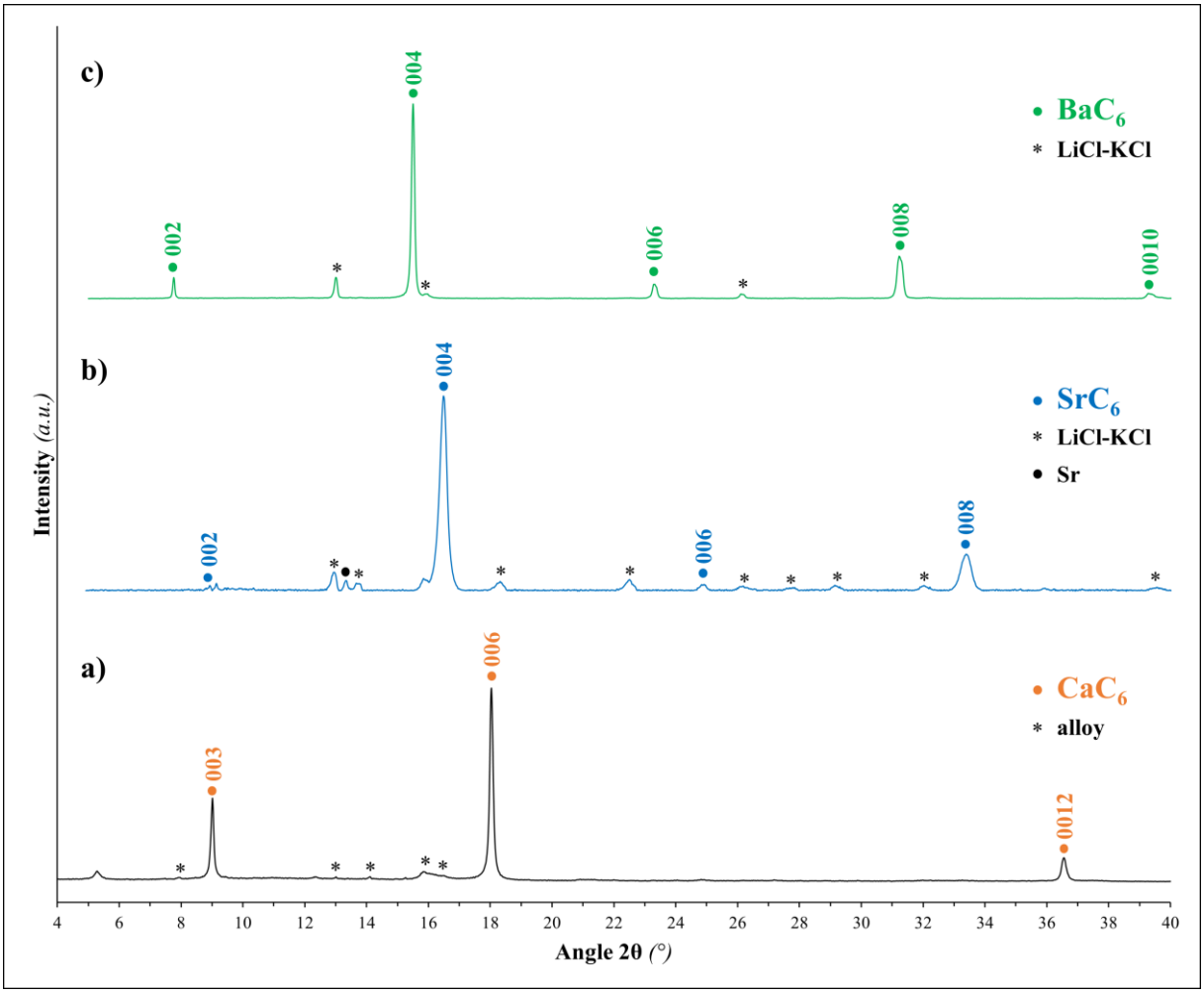

Fig. 1. 00*l* X-ray diffractograms ($\lambda_{MoK\alpha1}$ = 70.926 nm) of a) CaC_6, b) SrC_6 and c) BaC_6.

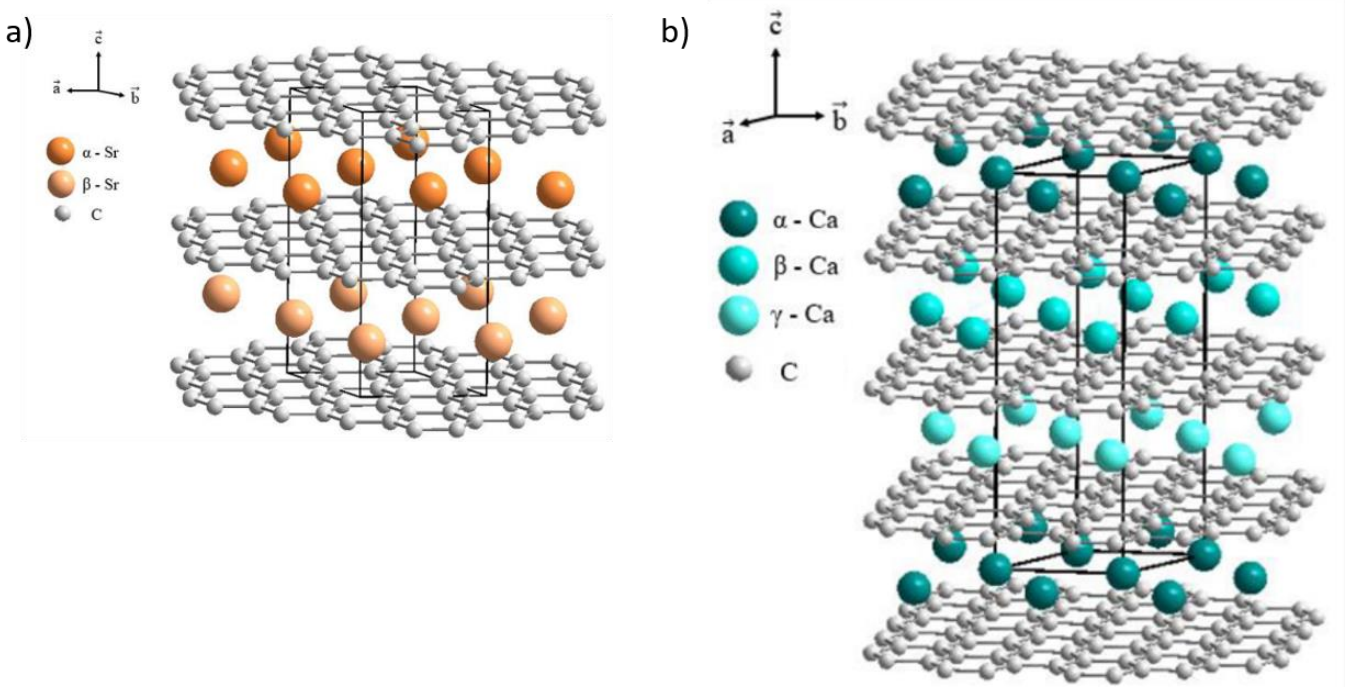

Fig. 2. a) Hexagonal unit cell ($P6_3/mmc$ space group) of BaC_6 and SrC_6; b) Rhombohedral unit cell (R-3m space group) of CaC_6.

In spite of the difference in the 3D crystal structure of these three MC_6 compounds, their 2D unit cells are the same (Fig. 3). This "hexal" lattice is commensurate with that of graphite. However, slight differences in their a parameter are revealed due to the charge transfer.

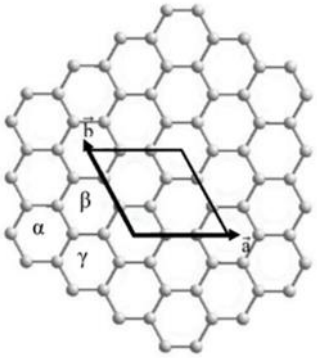

Fig. 3. 2D "hexal" unit cell of MC_6 compounds (M = Ba, Sr, Ca).

*hk*0 diffractograms in the 32-34 2θ° range are presented Fig. 4 with a focus on the 300 reflection of the MC_6 compounds, close to that of the 220 one of diamond. Using diamond powder as an internal standard during the recording of *hk*0 reflections, the accurate position of the 300 peak can be determined, and then the corresponding value of d_{300} can be calculated, leading to the a lattice parameter. In Table 1 we report the values of the charge transfer from the intercalated sheets to the graphene layers for each compound as calculated by using the Pietronero-Strässler formula [3]. The higher the a parameter is, the greater the charge transfer is: it slightly increases from BaC_6 to SrC_6 and more intensively to CaC_6, for which it attains the highest, *i.e.* about 0.095 electron per carbon atom.

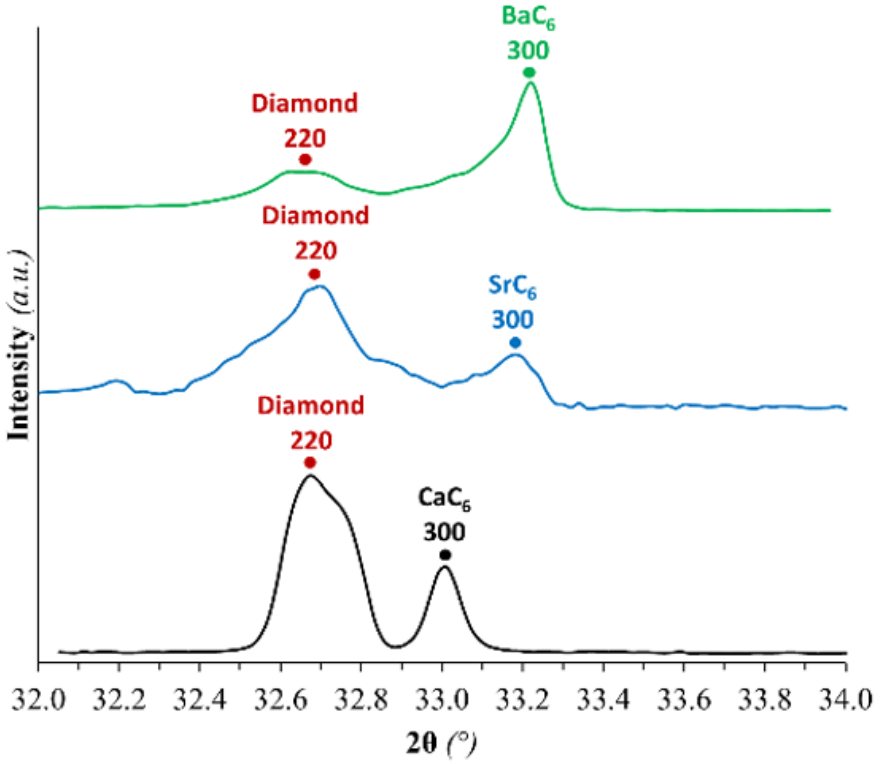

Fig. 4. *hk*0 X-ray diffraction patterns ($\lambda_{MoK\alpha1}$ = 70.926 nm) of the MC_6 compounds (M = Ba, Sr, Ca) showing their 300 reflection. The diamond 220 reflection is reported as an internal standard reference.

Table 1: Crystallographic data and charge transfer values of CaC_6, SrC_6 and BaC_6.

GIC	***a*** *(pm)*	***2ϑ*** *(°)*	***d_{300}*** *(pm)*	***$d_{C\text{-}C}$*** *(pm)*	***$\Delta d_{C\text{-}C}$*** *(pm)*	***f_C*** ***(e^-/C)***	***$d_{C\text{-}AE}$*** ***(pm)***	***d_i (pm)***
C_{gr}	***245.95***	***33.52***	***122.98 (d_{110})***	***142.00***	-	-	-	***335.0 (d_{002})***
BaC_6	429.13	33.27	123.88	143.04	1.04	0.051	263.5	527.0
SrC_6	430.82	33.18	124.20	143.61	1.61	0.075	247.0	494.0
CaC_6	432.39	33.01	124.82	144.13	2.13	0.095	225.5	451.0

3.2 Evolution of Raman spectra with the intercalated alkaline earth metal

Raman spectroscopy measurements on BaC_6, SrC_6 and CaC_6 were performed on the full available frequency range and are plotted in figure 5. Between 2600 and 2800 cm^{-1}, the 2D band peak normally present in graphite and GIC with stage greater than one is totally absent in this case (Fig. 5-c). Since such peak is due to *c*-axis graphene layers stacking phonon modes, this finding does confirm a successful bulk intercalation process of a first stage GIC.

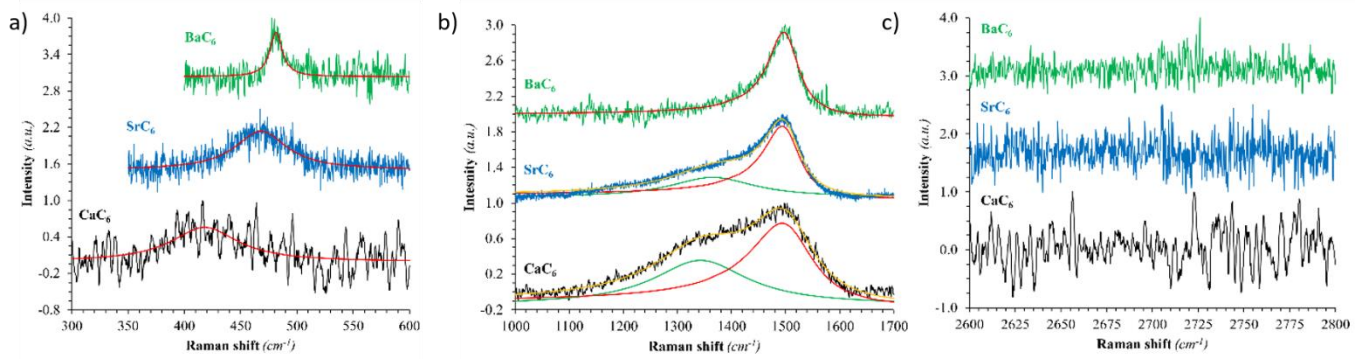

Fig. 5. Raman spectra (λ = 632.8 nm) of the MC_6 compounds (M = Ba, Sr, Ca): (a) the C_z band region. Each spectrum can be fitted with a Lorentzian function (red line). (b) C_{xy} band region (yellow: fitting). Red line corresponds to a BWF function fit and the green line represents the contribution of a Lorentzian-like D band. (c) the graphite 2D band region.

Panels 5-a and 5-b represent the Raman spectra focused on the 300-600 cm^{-1} and 1000-1700 cm^{-1} ranges corresponding to C_z and C_{xy} vibrational modes, respectively. We remark that the C_z band is fitted by a Lorentzian function whereas the C_{xy} one is fitted by the sum of a Breit-Wigner-Fano function (BWF) around 1500 cm^{-1}, and a Lorentzian one about 1300 cm^{-1} corresponding to the *D*-band, which appears only on SrC_6 and CaC_6 spectra. Since Raman spectroscopy probing depth is not more than some µm, such contribution normally associated to structural disorder, generally indicates the presence of small amount of oxidation at sample surface likely occurred during the transfer of these samples for Raman experiments. The presence of characteristic C_z and C_{xy} phonon modes confirm first stage GIC, in agreement with results obtained by XRD. All fitting parameters of C_z et C_{xy} peaks are reported in Table 2. It should be noted that the C_z mode shifts to lower wave number passing from BaC_6 to CaC_6 together with an increase in the line bandwidth: such behaviour is associated to a bond weakening due to the filling of the antibonding π* state, *i.e.* the charge transfer and to a strong electron-phonon coupling respectively. Similarly, the FWHM of the C_{xy} band also increases from BaC_6 to CaC_6 but no appreciable displacement of the peak position is observed nor a sizable variation of the *q*-parameter representing the degree of asymmetry of the BWF peak, both

effects being likely due the strong electron-phonon coupling. Both the C_z position and C_{xy} FWHM values determined in the present study are in good agreement with the ones presented in ref. [15]. The small differences (a few %) are probably due to the different quality of the samples. Indeed, the samples studied in Ref. [15] were prepared by the solid-gas method, during which the intercalation generally occurs only on the sample surface. On the other hand, the molten alloy and molten salts techniques give fully bulk intercalated samples [21] [25] [26] [27] [28].

Table 2: Fitted parameters of C_z and C_{xy} vibrational modes for Raman spectra recorded on MC_6 GIC. The phonon frequencies calculated in the adiabatic (ad.) approximation are also reported (see paragraph 3.3 for details).

	BaC_6	SrC_6	CaC_6
C_z vibrational mode			
DFT-ad. *(cm^{-1})*	479.9	454.9	434.2
Raman			
Position *(cm^{-1})*	481	467	418
FWHM *(cm^{-1})*	13.2	55.0	72.2
C_{xy} vibrational mode			
DFT-ad. *(cm^{-1})*	1495	1465	1456
Position *(cm^{-1})*	1501	1501	1504
FWHM *(cm^{-1})*	68	85	148
q-asymmetry	-7.0	-6.3	-6.4

The evolution of the interlayer distance is strongly correlated with the position of the C_z band and the C_{xy} FWHM in full agreement with the experimental results presented in ref. [15]. On the contrary, the position of the C_{xy} phonon mode is unaffected by the intercalant species and the interlayer distance because of strong electron-phonon coupling which prevents the electron from an immediate response due to vibrating ions (non-adiabatic limit). Indeed, as the interlayer distance decreases, the charge transfer between the intercalant atoms and graphene layers is expected to increase [29]. The non-adiabatic effects are reinforced with the increase of the π^* charge transfer causing an attenuation of the phonon lifetime which increases the broadening of the C_{xy} peak *i.e.* the FWHM parameter of C_{xy} band passing from BaC_6 to CaC_6. Finally, the Raman spectroscopy confirms the evolution of the electron charge transfer as detected by XRD measurements.

3.3 Modeling of charge transfer in the alkaline earth metal GIC

In order to understand and confirm the above experimental evidences, we calculated the structural, electronic and dynamical properties of the studied GIC by first-principles DFT calculations using the QUANTUM-ESPRESSO code [30] [31] and the generalized gradient approximation in the PBE parametrization [32] [26]. We used norm-conserving pseudopotential with valence configuration $2s^2 2p^2$ for C, $3s^2 3p^6 4s^2$ for Ca, $4s^2 4p^6 5s^2$ for Sr and $5s^2 5p^6 6s^2$ for Ba. The wave functions and the charge density are expanded using a 80 and a 320 Ry cutoff energy, respectively. To evaluate the charge transfer, δ, from M (M= Ca, Sr, Ba) to C_6, we divided GIC in different regions containing the graphene and the intercalate layers. The different regions were determined calculating the planar average, $\bar{\rho}_{xy}(z) = \iint \rho(x,y,z)dz$, interpolating the charge density on a dense real space grid (50000 points per unit cell) to converge the results, and then identifying the planes in which its derivative with respect to z is zero. These planes delimit the separation between C_6 and M. Phonons at Γ-point are calculated using density functional perturbation theory in the linear response approach [30] [31].

We used the measured experimental lattice parameters for all the compounds (Tab. 1). For CaC_6, although it crystallises in a R-3m space group, we performed the calculation using a $P6_3/mmc$ unit cell, considering that the structures differ only for the *c*-axis stacking of the intercalate and to have a clearer direct comparison of the electronic properties with the other compounds. Indeed, we verified that there are not differences in the calculated electronic structure.

First of all, we analysed the calculated electronic structure and the charge density profiles of MC_6. The band structure along the high symmetry lines of the Brillouin Zone are reported in Figure 6. In the $P6_3/mmc$ phase the graphene Dirac point is folded at Γ and splitted by the distortion induced by the reduced space group. The different intercalant atoms modify the energy position of the Dirac point with respect to the Fermi energy: in particular the Dirac point is shifted at higher energies (closer to the Fermi energy) in going from Ca to Ba.

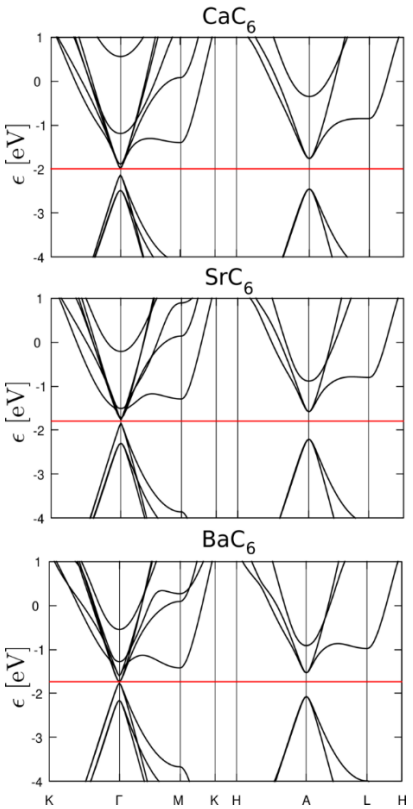

Fig. 6. Band structure for CaC_6, SrC_6, BaC_6 in a $P6_3/mmc$ unit cell. The zero of the energy is set to the Fermi energy. The red line indicated the energy position of the Dirac point.

The charge transfer can be measured calculating the planar average of the valence charge density $\bar{\rho}_{xy}$ as a function of z. In Figure 7 we plot $\bar{\rho}_{xy,MC_6} - \bar{\rho}_{xy,M} - \bar{\rho}_{xy,C_6}$, where $\bar{\rho}_{xy,M}$ $\left(\bar{\rho}_{xy,C_6}\right)$ are the planar averages calculated considering the same structure of the MC_6 compound removing the C_6 (M) layers, as a measure of the charge transfer between M and C_6 layers, for all the intercalants. Positive (negative) signs thus indicate charge accumulation (depletion) with respect to the constituent compounds. While for CaC_6 the charge accumulates between the graphene layers and the intercalated atom, in SrC_6 and BaC_6 a clear charge accumulation is present on the M atom, signalling a less effective charge transfer to the graphene layers. We remark that such behaviour agrees and explains the variation of the transferred charge per carbon atom as determined experimentally by XRD.

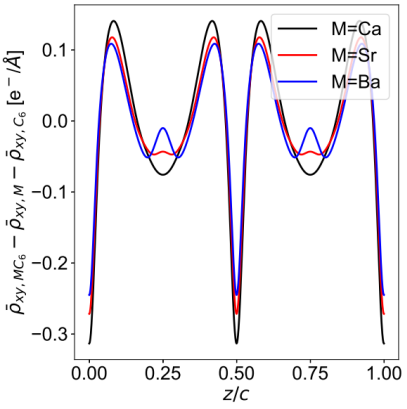

Fig. 7. Difference between the planar charge density of MC_6 and charge density of the M atom plus the charge density of the C_6 layers. The z is normalized with the c-axis unit cell parameter reported in Table 3.

We verified that increasing the charge transfer to the π^* bands weakens the interlayer bonds, producing a softening of the C_z frequency mode [29] as shown in Figure 8, in which we reported the variation of the C_z phonon frequency as a function of the calculated charge transfer, δ, from M to the C_6 layer. Such result is in full agreement with the variation of the phonon frequency with the intercalant atom as observed by Raman spectroscopy (Fig. 5-b). In detail, the softening of the C_z phonon frequency is determined by the charge transfer between intercalant atoms and graphene sheets, favoured by the lowering of the interlayer distance. The softening is caused by the weakening of the carbon bonds due to the filling of the antibonding π^* state, *i.e.* the charge transfer.

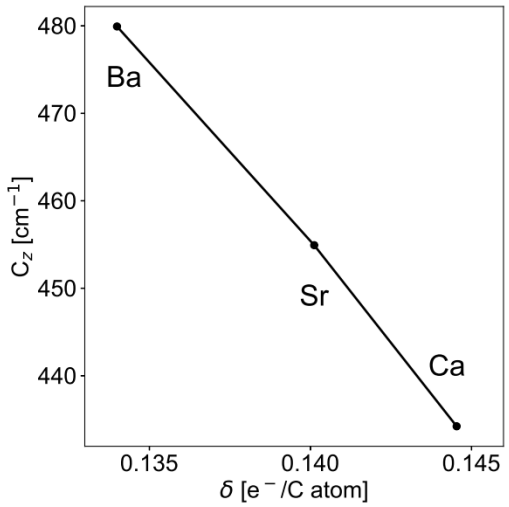

Fig. 8. Dependence of the frequency of the C_z mode on the charge transfer for the different intercalated compounds.

In Table 2, the calculated adiabatic phonon frequencies are compared with the experimental ones measured by Raman spectroscopy showing a general good agreement. It is worth to note that the discrepancy between the experimentally measured and the calculated C_{xy} phonon mode for CaC_6 can be attributed to non-adiabatic effects [33] that are particularly relevant in the case of Ca intercalant due to the strong electron-phonon coupling and they must be taken into account. Therefore, non-adiabatic calculation of the C_z and C_{xy} phonon frequencies in the case of CaC_6 compound were also performed within the time-dependent linear-response theory through Wannier interpolation as described in Ref. [33] [34]. The calculation confirms how the most affected phonon modes are the C_{xy}, which pass from 1456 cm^{-1} in the adiabatic approximation to 1538 cm^{-1} including non-adiabatic effects for the Ca atom. As expected, due to the lower frequency, non-adiabatic corrections do not affect appreciably the C_z modes.

4. Conclusion

In conclusion, we presented a detailed study of the mechanism of the charge transfer from the intercalant atoms to the carbon layers in alkaline-earth first stage GIC BaC_6, SrC_6 and CaC_6 by means of XRD and Raman spectroscopy measurements on high quality bulk intercalated samples and through detailed DFT calculations in both adiabatic and non-adiabatic limits. Thus, we were able to give a coherent picture that explains where, why and with which effects the intercalant valence electronic charge is transferred to the carbon planes passing from Ba to Ca atoms. Such picture does reinforce and further help the comprehension of superconductivity in first stage GIC.

References:

[1] Cahen S., Speyer L., Lagrange P., Hérold C., Topotactic Mechanisms Related to the Graphene Planes: Chemical Intercalation of Electron Donors into Graphite, Eur. J. Inorg. Chem., 2019, 2019, 4798-4806. https://doi.org/10.1002/ejic.201900758

[2] Nixon D. E., Parry G. S., The expansion of the carbon-carbon bond length in potassium graphites, J. Phys. C., Solid State Phys., 1969, 2, 1732. DOI 10.1088/0022-3719/2/10/305

[3] Pietronero L., Strässler S., Bond-Length Change as a Tool to Determine Charge Transfer and Electron-Phonon Coupling in Graphite Intercalation Compounds, Phys. Rev. Lett., 1981, 47, 593-596. https://doi.org/10.1103/PhysRevLett.47.593

[4] Emery N., Hérold C., d'Astuto M., Garcia V., Bellin Ch., Marêché J. F., Lagrange P., Loupias G., Superconductivity of Bulk CaC6, Phys. Rev. Lett., 2005, 087003. https://doi.org/10.1103/PhysRevLett.95.087003

[5] Kim J. S., Boeri L., O'Brien J. R., Razavi F. S., Kremer R. K., Superconductivity in Heavy Alkaline-Earth Intercalated Graphites, Phys. Rev. Lett., 2007, 99, 027001. https://doi.org/10.1103/PhysRevLett.99.027001

[6] Heguri S., Kobayashi M., Synthesis and physical properties of alkaline earth metal graphite compounds, J. Phys. Chem. Solids, 2010, 71, 572-574. https://doi.org/10.1016/j.jpcs.2009.12.039

[7] Hannay N.N., Geballe T.H., Matthias B.T., Andres K., Schmidt P., Mac Nair D., Superconductivity in Graphitic Compounds, Phys. Rev. Lett., 1965, 14, 225-226. https://doi.org/10.1103/PhysRevLett.14.225

[8] Calandra M., Mauri F., Origin of superconductivity of CaC6 and of other intercalated graphites, Phys. Stat. Sol. (b), 2006 , 243, 3458-3463. https://doi.org/10.1002/pssb.200669206

[9] Csányi G., Littlewood P. B., Nevidomskyy A. H., Pickard C. J., Simons B. D., The role of the interlayer state in the electronic structure of superconducting graphite intercalated compounds, Nature Phys., 2005, 1, 42-45. https://doi.org/10.1038/nphys119

[10] Calandra M., Mauri F., Possibility of superconductivity in graphite intercalated with alkaline earths investigated with density functional theory, Phys. Rev. B, 2006, 74, 094507. https://doi.org/10.1103/PhysRevB.74.094507

[11] Heguri S., Kawade N., Fujisawa T., Yamaguchi A., Sumiyama A., Tanigaki K., Mototada K., Superconductivity in the Graphite Intercalation Compound BaC6, Phys. Rev. Lett., 2015, 114, 247201. https://doi.org/10.1103/PhysRevLett.114.247201

[12] Nemanich R. J., Solin S. A., Guérard D., Raman scattering from intercalated donor compounds of graphite, Phys. Rev. B., 1977, 16, 2965-2972. https://doi.org/10.1103/PhysRevB.16.2965

[13] Solin S. A., Caswell N., Raman scattering from alkali graphite intercalation compounds, J. Raman Spectrosc., 1981, 10, 129-135. https://doi.org/10.1002/jrs.1250100124

[14] Mialitsin A., Kim, J. S., Kremer R. K., Blumberg G., Raman scattering from the CaC6 superconductor in the presence of disorder, Phys. Rev. B, 2009, 79, 064503. https://doi.org/10.1103/PhysRevB.79.064503

[15] Dean M. P. M., Howard C. A., Saxena S. S., Ellerby M., Nonadiabatic phonons within the doped graphene layers of XC6 compounds, Phys. Rev. B, 2010, 81, 045405. https://doi.org/10.1103/PhysRevB.81.045405

[16] Chacón-Torres J. C., Pichler T., Defect modulated Raman response of KC8 single crystals, Phys. Status Solidi B, 2011, 248, 2744-2747. https://doi.org/10.1002/pssb.201100135

[17] Chacón-Torres J. C., Ganin A. Y., Rosseinsky M. J., Pichler T., Raman response of stage-1 graphite intercalation compounds revisited, Phys. Rev. B, 2012, 86, 075406. https://doi.org/10.1103/PhysRevB.86.075406

[18] Emery N., Hérold C., Lagrange P., ADVANCES IN SUPERCONDUCTING INTERCALATED GRAPHITE, In: Superconductivity Research Advances, Nova Science Publishers, 2007, 261, pp3-52. ISBN: 978-1-60021-691-6

[19] Saitta A. M., Lazzeri M., Calandra M., Mauri F., Giant Nonadiabatic Effects in Layer Metals: Raman Spectra of Intercalated Graphite Explained Phys. Rev. Lett., 2008, 100, 226401. https://doi.org/10.1103/PhysRevLett.100.226401

[20] Hlinka J., Gregora I., Pokorny J., Hérold C., Emery N., Marêché J.F., Lagrange P., Lattice dynamics of CaC6 by Raman spectroscopy, Phys. Rev. B, 2007, 76, 144512. https://doi.org/10.1103/PhysRevB.76.144512

[21] Emery N., Hérold C., Lagrange P., Structural study and crystal chemistry of the first stage calcium graphite intercalation compound, J. Solid State Chem., 2005, 178, 2947-2952. https://doi.org/10.1016/j.jssc.2005.05.031

[22] Pruvost S., Hérold C., Hérold A., Lagrange P., On the great difficulty of intercalating lithium with a second element into graphite, Carbon, 2003, 41, 1281-1289. https://doi.org/10.1016/S0008-6223(03)00074-5

[23] Emery N., Hérold C., Lagrange P., The synthesis of binary metal-graphite intercalation compounds using molten lithium alloys, Carbon, 2008, 46, 72-75. https://doi.org/10.1016/j.carbon.2007.10.039

[24] Hagiwara R., Ito M., Ito Y., Graphite intercalation compounds of lanthanide metals prepared in molten chlorid, Carbon, 1996, 34, 1591-1593. https://doi.org/10.1016/S0008-6223(96)00109-1

[25] Bolmont M., Cahen S., Fauchard M., Guillot R., Medjahdi G., Berger P., Lamura G., Lagrange P., Hérold C., LiCl-KCl eutectic molten salt as an original and efficient medium to intercalate metals into graphite: Case of europium, Carbon, 2018, 133, 379-383. https://doi.org/10.1016/j.carbon.2018.03.015

[26] Fauchard M., Cahen S., Bolmont M., Medjahdi G., Lagrange P., Hérold C., An efficient medium to intercalate metals into graphite: LiCl-KCl molten salts, Carbon, 2019, 144, 171-176. https://doi.org/10.1016/j.carbon.2018.12.014

[27] El Hajj I., Speyer L., Cahen S., Lagrange P., Medjahdi G., Hérold C., Crystal structure of first stage strontium-graphite intercalation compound, Carbon, 2020, 168, 732-736. https://doi.org/10.1016/j.carbon.2020.05.102

[28] El Hajj I., Speyer L., Cahen S., Herbuvaux L., Lagrange P., Medjahdi G., Hérold C., Intercalation of barium into graphite by molten salts method: Synthesis of massive samples for crystal structure determination of BaC6, Carbon, 2022, 431-436. https://doi.org/10.1016/j.carbon.2021.09.073

[29] Boeri L., Bachelet G. B., Giantomassi M., Andersen O. K., Electron-phonon interaction in graphite intercalation compounds, Phys. Rev. B, 2007, 76, 064510. https://doi.org/10.1103/PhysRevB.76.064510

[30] Giannozzi P., Baroni S., Bonini N., Calandra M., Car R., Cavazzoni C et al., QUANTUM ESPRESSO: a modular and open-source software project for quantum simulations of materials, J. Phys. Condens. Mat., 2009, 21, 395502. DOI: 10.1088/0953-8984/21/39/395502

[31] Giannozzi P., Andreussi O., Brumme T., Bunau O., Buongiorni Nardelli M., Calandra M. et al., Advanced capabilities for materials modelling with Quantum ESPRESSO, J. Phys. Condens. Mat., 2017, 29, 465901. DOI: 10.1088/1361-648X/aa8f79

[32] Perdew J. P., Burke K., Ernzerhof M., Generalized Gradient Approximation Made Simple, Phys. Rev. Lett., 1996, 77, 3865. https://doi.org/10.1103/PhysRevLett.77.3865

[33] Calandra M., Profeta G., Mauri F., Adiabatic and nonadiabatic phonon dispersion in a Wannier function approach, Phys. Rev. B, 2010, 82, 165111. https://doi.org/10.1103/PhysRevB.82.165111

[34] Marini G., Marchese G., Profeta G., Sjakste J., Macheda F., Vast N. et al., epiq: An open-source software for the calculation of electron-phonon interaction related properties, Comput. Phys. Commun., 2024, 295, 108950. https://doi.org/10.1016/j.cpc.2023.108950